

Strike point splitting induced by the application of magnetic perturbations on MAST

P. Cahyna^{a,1,*}, M. Peterka^a, A. Kirk^b, A. Thornton^b, J. Harrison^b, D. Muir^b,
R. Panek^a, the MAST team

^a*Institute of Plasma Physics, AS CR, v.v.i., Association EURATOM/IPP.CR, Za
Slovankou 3, 182 00 Prague, Czech Republic*

^b*EURATOM/CCFE Fusion Association, Culham Science Centre, Abingdon, Oxon, OX14
3DB, UK*

Abstract

Divertor strike point splitting induced by resonant magnetic perturbations (RMPs) has been observed on MAST for a variety of RMP configurations in a plasma scenario with $I_p = 750$ kA where those configurations all have similar resonant components. Complementary measurements have been obtained with divertor Langmuir probes and an infrared camera. Clear splitting consistently appears in this scenario only in the even configuration of the perturbation coils, similarly to the density pump-out. These results present a challenge for models of plasma response to RMPs.

Keywords: Plasma properties, Plasma-Materials Interaction

*Corresponding author

Email address: cahyna@ipp.cas.cz (P. Cahyna)

¹Presenting author

1. Introduction

The application of resonant magnetic perturbations (RMPs) to tokamak plasma with an X-point is expected to result in formation of a 3-D structure of magnetic field lines — the homoclinic tangle, replacing the original separatrix [1]. This should in turn result in formation of spiralling structures of fluxes (footprints) on the divertor as parallel transport carries particles and energy along the field lines inside the tangle from the core plasma directly to the divertor plates. Such perturbations are used for ELM control and foreseen for this use on ITER [2], and during the ELM control experiments such structures are indeed observed. The observation is usually performed on a single toroidal location on the divertor along a radial profile. The strike point is then observed to split into multiple peaks which correspond to the intersections of the diagnostic line of sight with the footprints. The experimental evidence for the formation of footprints has been mixed though. Generally the effect is more consistently observed in L-mode than in H-mode [3, 4], and the observations also depend on the quantity being measured: heat flux, measured by the infrared (IR) camera, shows much less clear splitting than visible light emission in DIII-D low-collisionality H-mode discharges [4] (results are again different for high collisionality [5]).

From the theoretical point of view the interesting feature of divertor footprints is that they are determined by the same quantities as the resonant perturbation modes which determine the width of magnetic islands and thus the transition to stochastic regime of field lines — the Melnikov [6, 7] or Poincaré [8] integrals. One of the open questions of the RMP technique is to what extent the plasma screens the resonant modes and thus reduces the edge stochastic layer to much lesser width than predicted by vacuum calculations. Such screening is predicted by extended MHD [9] and kinetic [10] models especially for H-mode due to strong gradients and flows in the pedestal. Footprints are then predicted to be significantly reduced in comparison to results based on vacuum field [11] when screening is introduced in the model. The observations of footprints thus provide a valuable test for screening models — the differences in experimental results may be partly due to differences in plasma response [3].

Significant number of experiments with RMPs have been performed on the MAST tokamak [12, 13, 14] since the installation of the in-vessel RMP coils [15]. One notable effect of RMP application on MAST is the density pump-out in L-mode. It is remarkable that in a scenario with 750 kA of plasma current the pitch angle of edge field lines is such that the odd and even configuration of the perturbation field have similar resonant components. This results in an almost identical Chirikov factor profile, however the density pump-out has been observed in the even configuration only [14]. The pump-out thus can not be explained by any mechanism relying purely on the formation of a stochastic layer in the vacuum field. Even introduction of screening can hardly explain the difference, as the screening results from an interplay between the resonant modes, plasma flows and other plasma parameters (resistivity, viscosity), which are here same or similar for the even and odd configurations in the same plasma

scenario. One possibility proposed in [14] is that the plasma response has a different form for even and odd perturbation, as measured by the displacement calculated by the MHD model MARS-F. In any case, thanks to the unexpected results, this scenario represents an important testbed of plasma response models. At the same time the fact that it is in L-mode simplifies modelling since it does not need to take into account the strong gradients and flows in H-mode.

Due to the importance of the aforementioned experiments for the understanding of plasma response to RMPs and the ability of divertor footprints to reveal details of the magnetic field we present in this paper an analysis of the strike point data available for these shots. As in the previous reports on divertor footprint observations on MAST [3, 12] we used an IR camera to measure temperature and infer heat flux to the divertor targets. In addition we use here for the first time on MAST the divertor Langmuir probe measurements to enlarge the base of available data, following the example of DIII-D [16].

2. Experimental setup and methods

The plasma scenario used in all the shots presented here is a double-null, L-mode plasma with a current of 750 kA. The set of perturbation coils was described in [15]. The coils are wired in an $n = 3$ configuration, either even or odd parity. For each parity there are two possible phases, labeled as 0° and 60° , yielding four possible configurations in total. In all the shots studied here the current in the RMP coils had the same time evolution. During a shot the strike point position is evolving due to the influence of the changing field of the central solenoid. The data collected from the divertor at a given toroidal position are a function of two variables: time and radial position on the divertor plate. If we plot this function we see the motion of the strike point and features associated with it, such as the secondary maxima due to strike point splitting. In contrast there can be patterns due to irregularities in the divertor surface, or in the case of probes, to one probe having a systematic error. Those patterns are static and thus the motion of strike points allows us to distinguish them from the real strike point splitting.

The strike point on the lower divertor was observed by an IR camera with a wavelength range of 4.5 to 5.0 μm and temporal resolution of 1250 μs . The camera was zoomed on a radial band on the divertor with a size of 320×96 pixels, the spatial resolution was 1 mm. From the measured temperature of the divertor plate the incoming heat flux is estimated.

In addition there are six arrays of Langmuir probes in the divertor plates, three in the lower and three in the upper divertor at toroidal locations with toroidal angles of $\varphi = 233^\circ, 288^\circ, 333^\circ$. Distance between consecutive probes is 9.23 mm. The probes are being continually swept and the I-V characteristics is measured, which is then fitted in order to obtain the floating potential V_{float} , ion saturation current J_{sat} , electron temperature T_e and an estimate of the incoming power. Each voltage sweep takes 65 μs but due to multiplexing each probe is only swept once every 1.04 ms. The spatial resolution of the probes is rather low for measuring structures such as the divertor footprints. The

resolution can be significantly enhanced by using the strike point motion which causes a given probe to measure points with varying distance from the primary strike point as the whole footprint structure is moving across it. To exploit this we divide the divertor space in bins with fixed width and distance from the primary strike point whose position is determined by equilibrium reconstruction (using the EFIT code) and in every bin we perform an averaging over the values which fall into it during the time evolution. We have been using a bin width of 6.5 mm. It would be possible to use even smaller bins to further improve the radial resolution, but due to fairly significant noise in the data choosing larger bins produces data of better quality thanks to averaging of more values. This technique requires the relative position of the EFIT prediction and the actual strike point to be unchanging during a shot, although an agreement on the absolute position is not necessary.

This method on the other hand significantly reduces the time resolution. We have been using only two time windows for averaging, giving us two time points. The first window is for times from 0.18 s to 0.22 s and the second one from 0.22 s to 0.24 s (the windows are shown as color bars in Fig. 3). The boundary (0.22 s) was chosen as at this time structures usually start to appear (see Fig. 3) and the current in the RMP coils nearly reaches its maximum value (*ibid.*).

3. Results

The list of shots discussed below and shown in the figures is given in table 1. The IR camera observes in many cases a clearly recognizable splitting of the strike point after the perturbation has been switched on. In some cases however there is no or almost undistinguishable splitting. In other cases there is a clearly visible peak about 4 cm away from the strike line (Fig. 1). Its position agrees with the position of the magnetic footprint predicted by vacuum modelling. The analysis of the available shots reveals that the even parity 60° phase shots consistently exhibit the former result while the even parity 0° phase shots the latter. One exception is the shot 22625 which had opposite current and toroidal field than the other shots and in which the perturbation was of an even parity 60° phase. Here the result is similar to the shots with 0° phase (splitting with a clearly defined secondary peak at about 4 cm outside the primary one, Fig. 2). There had been only few shots in odd parity. The shots with 60° phase did not show any splitting (Fig. 2), however the camera was not zoomed so the resolution was inferior to the other shots. The shot with 0° phase had the same camera setup (zoomed) as most of the other shots. Here splitting was not observed either (Fig. 2).

The time evolution of the floating potential V_{float} from probes in all the available six sectors for the shot 25941 (even parity 60° phase) is shown in Fig. 3 together with the evolution of strike points predicted by EFIT and the time trace of the current in the perturbation coils I_{RMP} . The predicted strike point follows the same path as the actual maxima and minima of V_{float} , however we see that the absolute position of predicted strike point is not correct and

moreover the displacement is not the same in different sectors. The appearance of multiple bands when the coils are switched on can be clearly seen, despite the lack of clear splitting in IR images for this shot. Note that the separation of the bands is different in each sector. The profile of V_{float} is rather different in every sector even before the coils are switched on and is not monotonic with increasing distance from the strike points.

Figure 4 shows the profiles of the power flux averaged over two time windows before (black lines) and after (red lines) the coils are switched on in four sectors. (In the remaining two the data are very noisy and not usable.) Shots with maximum coil current in different configurations and reference shots with zero coil current are compared. The profiles are shown as a function of distance from the strike point predicted by EFIT, as described above. The shots with odd parity configuration are from another experimental campaign than the others, here changes in both the EFIT prediction and the actual strike points position result together in a large displacement of the profile.

4. Discussion

IR camera and divertor probes can both reveal strike point splitting and both have advantages and disadvantages. The IR camera has the advantage of superior space resolution and less noise, however it usually observes only one location and more observation points, while desirable due to the 3D nature of the effect, are difficult to achieve due to the significant price of the equipment. For this reason it is advisable to have also divertor probe arrays when feasible. We saw that the additional data from divertor probes enabled us to confirm the existence of splitting in a scenario (even 60° phase) where the camera did not detect it. The disadvantage of probes is the much inferior quality of their data. The clearest picture of strike point splitting was obtained using the V_{float} measurement. It is remarkable that there is a significant drop of the minimum of the floating potential on the lower probe arrays, reminiscent of the DIII-D results [16] and possibly indicating a presence of field lines connected to the core plasma. The floating potential observations are only qualitative though, as the dependence of V_{float} on the distance from the strike point is complicated and moreover different for each probe array. For this reason we have been using the power measurements, which show a simple exponential decrease with the distance from the strike points. This enables us to detect the effect of perturbation coils even in cases where there are no clear secondary peaks but the profile just broadens. The power measurements have much more noise than the V_{float} measurements, which are remarkably clean even in the two sectors where the power (and J_{sat} , T_e) data are too noisy to be useful. To eliminate the noise and systematic errors and increase the spatial resolution time averaging has been useful. The resulting profiles show large fluctuations at the peak, but the exponential decrease outside the strike point is remarkably smooth and very precisely overlaps for different shots before the coils are switched on and also in reference shots without perturbation. We can thus claim that the averaged profiles have negligible error and the observed profile broadening in cases with

perturbation is a real effect. The probes have also the advantage of being fixed, while the camera set-up can be changed or the camera can be removed according to the needs of the experiments. In principle, if all the auxiliary equipment (power supplies, amplifiers) remains identical, the probes can provide repeatable and comparable measurements.

The results show no clear splitting in odd configuration. To show that this is a consequence of the actual divertor footprints being small or absent it is necessary to compare several experimental profiles and coil configurations. For the even parity, in the 60° phase no significant splitting was observed either on the IR camera, in contrast with the 0° phase. The explication may be that the phase change rotates the footprints from the camera view. To prove that this is the case (rather than footprints being absent) one can use the probe data, which show actually more clear splitting in the 60° phase. This is supported by the fact that with an opposite plasma current and toroidal field the footprints were clearly seen on camera. It can be shown that a reversal of both the poloidal and toroidal fields is for the footprint geometry equivalent to a reversal of the perturbation phase. The position of peaks measured by probes is different for both phases and for different toroidal sectors. The latter difference is in agreement with the 3D nature of the footprints. As the negative result for the odd configuration was confirmed for both phases on both the camera and probes, we can confidently claim that the footprints are absent or significantly smaller than in the even configuration. In the future we will investigate if this difference may be due to the same difference in plasma response, as calculated by MARS-F, that was found to correlate with the density pump-out. If this were not the case then clearly the cause of the differences between odd and even parity should be looked for elsewhere.

5. Acknowledgements

Discussions with E. Nardon are highly appreciated. This work, part-funded by the European Communities under the contracts of Association between EURATOM and IPP.CR and CCFE, was carried out within the framework of the European Fusion Development Agreement. The views and opinions expressed herein do not necessarily reflect those of the European Commission. This work was also part-funded by the Grant Agency of the Czech Republic under grant P205/11/2341, MSMT CR #7G10072 and the RCUK Energy Programme under grant EP/I501045.

Shot	I_{RMP}	parity	phase	note
22625	1.4 kA	even	60°	reversed I_p and B_T
25941	1.4 kA	even	60°	
25953	0 kA	N/A	N/A	
25965	1.4 kA	even	0°	
25056	0 kA	N/A	N/A	
25057	1.4 kA	odd	60°	
27652	1.4 kA	odd	0°	

Table 1: List of shots used in this paper.

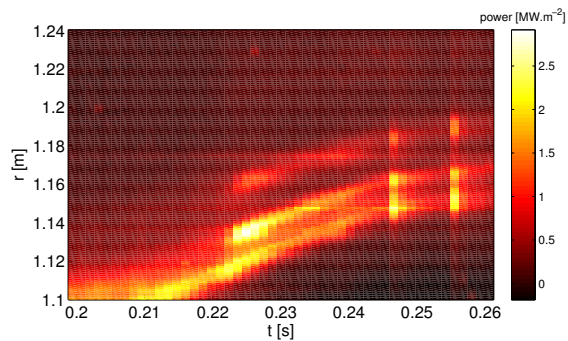


Figure 1: Time dependence of the heat flux profile to the divertor target measured by the IR camera for shot 25965.

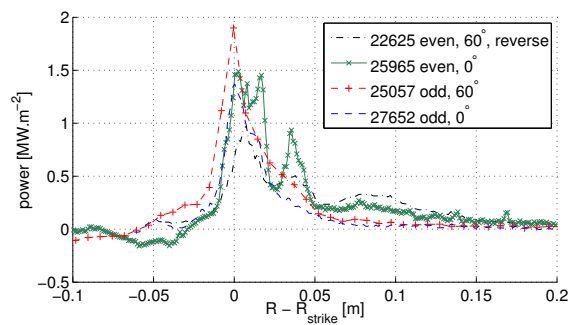


Figure 2: Heat flux profiles to the divertor target measured by the IR camera as a function of distance from the primary strike point for several shots at $I_{\text{RMP}} = 1.4$ kA at time $t = 0.24$ s.

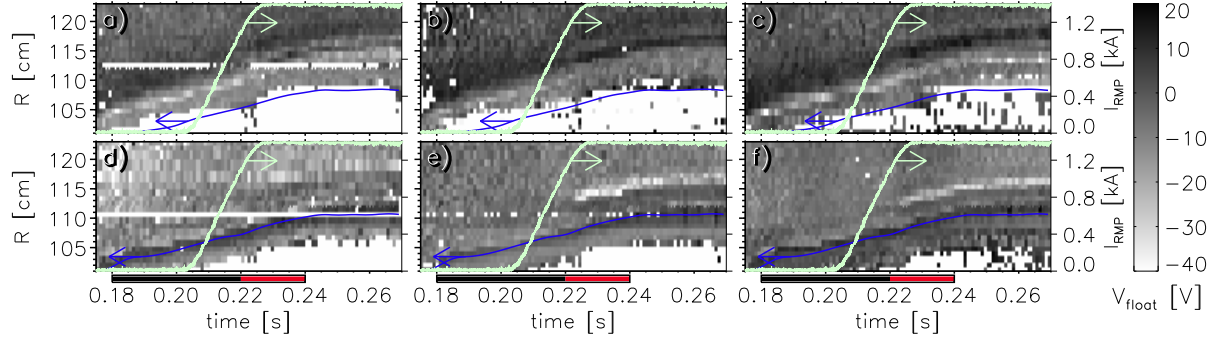


Figure 3: Time dependence of V_{float} on all the sectors of divertor probes during the shot 25941. a) – c) upper sectors, d) – f) lower sectors. Blue line: position of the strike point as calculated by EFIT (R_{EFIT}). Cyan line: current in the perturbation coils I_{RMP} , with a maximum of 1.4 kA. Black and red bands below the graph indicate the time windows used for averaging in the following figures.

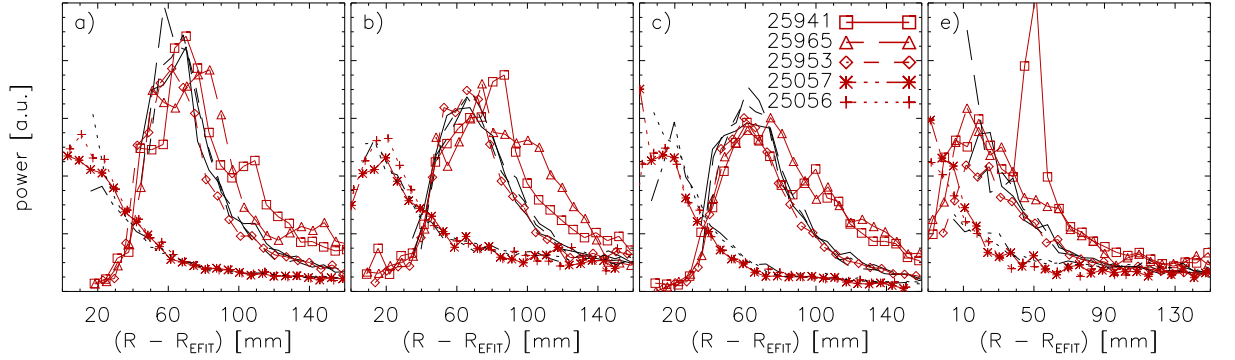


Figure 4: Comparison of heat flux profiles measured by the divertor probes for various perturbation coil configurations. Sectors are labeled according to Fig. 3. Black lines without symbols: time window before $t = 0.22$ s, red lines with symbols: time window after $t = 0.22$ s. Line styles distinguish shots and have the same meaning for black and red lines.

References

- [1] T. E. Evans, et al., *Journal of Physics: Conference Series* **7** (2005) 174–190.
- [2] P. R. Thomas, in *Fusion Energy 2008 (Proc. 22nd Int. Conf. Geneva)*, (Vienna: IAEA), 2008 CD-ROM file IT/1-5 and <http://www-naweb.iaea.org/napc/physics/FEC/FEC2008/html/index.htm>.
- [3] E. Nardon, et al., *Journal of Nuclear Materials* **415** (2011) S914 – S917.
- [4] O. Schmitz, et al., *Journal of Nuclear Materials* **415** (2011) S886 – S893.
- [5] M. Jakubowski, et al., *Nuclear Fusion* **49** (2009) 095013.
- [6] I. Joseph, et al., *Nuclear Fusion* **48** (2008) 045009.
- [7] P. Cahyna, E. Nardon, *Resonant magnetic perturbations and divertor footprints in poloidally diverted tokamaks* (2010), [arXiv:1005.3663](https://arxiv.org/abs/1005.3663)[physics.plasm-ph].
- [8] S. S. Abdullaev, et al., *Phys. Plasmas* **15** (2008) 042508.
- [9] E. Nardon, et al., *Nuclear Fusion* **50** (2010) 034002.
- [10] M. F. Heyn, et al., *Nuclear Fusion* **48** (2008) 024005.
- [11] P. Cahyna, et al., *Journal of Nuclear Materials* **415** (2011) S927 – S931, [arXiv:1012.4015](https://arxiv.org/abs/1012.4015)[physics.plasm-ph].
- [12] E. Nardon, et al., *Plasma Physics and Controlled Fusion* **51** (2009) 124010.
- [13] A. Kirk, et al., *Nuclear Fusion* **50** (2010) 034008.
- [14] A. Kirk, et al., *Plasma Physics and Controlled Fusion* **53** (2011) 065011.
- [15] E. Nardon, et al., *Journal of Nuclear Materials* **390-391** (2009) 773 – 776.
- [16] J. Watkins, et al., *Journal of Nuclear Materials* **390-391** (2009) 839 – 842.